Ocean Engineering 74 (2013) 37–47

Contents lists available at ScienceDirect

Ocean Engineering

journal homepage: www.elsevier.com/locate/oceaneng

High order force components of a near-wall circular cylinder oscillating in transverse direction in a steady current

Ying Chen, Shixiao Fu*, Yuwang Xu, Dixia Fan

State Key Laboratory of Ocean Engineering, Shanghai Jiao Tong University, Shanghai 200240, China

ARTICLE INFO

Article history:
Received 23 April 2013
Accepted 12 September 2013
Available online 16 October 2013

Keywords:
Pipeline
Forced oscillation
High-order hydrodynamic coefficients
Vortex-induced vibration

ABSTRACT

In the study described in this paper, the drag and lift forces on a circular cylinder undergoing forced oscillation in the transverse direction near a wall were experimentally investigated in a towing tank at a Reynolds number of 2×10^5. The first four orders of the components of the oscillating drag and lift forces were calculated. The effects of the gap ratio, oscillation frequency, and oscillation amplitude were studied, with particular emphasis on the influence of the nearby wall on the high-order force components. A rigid cylinder was placed near a flat plate, which was used to simulate the seabed, and was towed forward in the water together with the flat plate. The cylinder was forced into sinusoidal oscillation in the cross-flow direction over a wide range of oscillation frequency and amplitude. The hydrodynamic drag and lift forces were measured by three-dimensional force transducers attached to the ends of the cylinder.

1. Introduction

Marine pipelines are widely used for oil and gas transportation. They are often laid directly on the seabed, largely because of economic factors. Although pipelines are designed to be laid on a compacted, solid foundation, free spans may form either because of unevenness of the seabed or because of local scour below the pipeline caused by long-term flow denudation. When exposed to the action of a flow, such a free span in a pipeline may undergo the phenomenon of vortex-induced vibration, which is important for the fatigue life of pipelines. The problem is made worse by high-order hydrodynamic forces, leading to nonlinearities in the vibration of the pipe, as described by Huang and Larsen (2010) and Wang et al. (2013). Such high-order lift and drag forces can aggravate fatigue damage. The problem of a pipeline with a free span can be simplified to the idea of a stationary or oscillating cylinder near a wall, subject to a steady current.

Many researchers have studied the hydrodynamics of a stationary cylinder near a wall at subcritical Reynolds numbers, such as Roshko et al. (1975), Bearman and Zdravkovich (1978), Buresti and Lanciotti (1992), Grass et al. (1984), Zdravkovich (1985), Lei et al. (1999), and Nishino et al. (2007). These studies focused on the variation of the lift and drag coefficients for different gap ratios G/D, where G is the distance between the cylinder and the wall and D is the diameter of the cylinder. However, the hydrodynamics can be totally changed when a pipeline undergoes vortex-induced vibration, as may be the case in practical engineering situations, so it is necessary to understand the hydrodynamics of oscillating cylinders.

Experiments on forced oscillation and self-excited oscillation of rigid cylinders are two of the most important methods for the study of the mechanism of vortex-induced vibration and for its prediction. In the case of forced oscillation, the cylinder is driven externally at a certain frequency and amplitude, rather than being driven by its wake. The primary purpose of such studies is to study the forces acting on the cylinder and the energy transfer between the moving cylinder and the flow, and to obtain detailed hydrodynamic coefficients. In the case of self-excited oscillation, the moving cylinder is driven entirely by the interaction between the wake and the cylinder body, and hence the wake patterns and therefore the kinematics of the cylinder are the focus of research.

There have been numerous studies using forced-oscillation experiments in the past few decades. The work of Bishop and Hassan (1964) was among the first forced-oscillation experiments, and they observed the phenomena of synchronization and a "jump" in the force and the phase angle at certain critical frequencies. Williamson and Roshko (1988) explained the "jump" using vortex-shedding patterns. Sarpkaya (1978) decomposed the lift force on the basis of the phase angle, which can describe the energy transfer between the fluid and the structure. Gopalkrishnan (1993) conducted a series of experiments and presented the results as contour maps, which provided hydrodynamic coefficients for semi-empirical models such as SHEAR7 and VIVANA. Sumer et al. (1994) studied the hydrodynamics of an

* Corresponding author. Tel.: +86 13501947087; fax: +86 21 34207050.
E-mail address: shixiao.fu@sjtu.edu.cn (S. Fu).

0029-8018/$ - see front matter © 2013 Elsevier Ltd. All rights reserved.
http://dx.doi.org/10.1016/j.oceaneng.2013.09.009

oscillating cylinder near a wall in a current and waves; this provided one of the few sets of observations and data for subsequent research on forced oscillation of a cylinder near a wall.

Actually, investigation on the self-excited oscillation cylinder near a wall is very rare. Recently, Zhao and Cheng (2011) and Wang et al. (2013) have studied the vortex-induced vibration of an elastically mounted cylinder near a plane wall using numerical and experimental methods, respectively. They found that vortex-induced vibration occurred even for a small initial gap ratio. Yang et al. (2007) conducted experiments focusing on the difference between the vibration of a pipe near an erodible soil, near a rigid boundary, and under wall-free conditions.

Carberry et al. (2005) pointed out that although the two kinds of experiments are conducted with different purposes, there are striking similarities in the wake modes (2S and 2P) and the phase angle of the lift force, and in both cases the wake undergoes a transition as lock-in occurs. Sarpkaya (2004) pointed out that the results of forced-oscillation tests on cylinders can be used to predict the response of an elastically mounted cylinder.

Nearly all of the forced-oscillation experiments mentioned above focused only on the second-order drag and the first-order lift, according to the decomposition of Sarpkaya (1978). Few researchers paid close attention to the nonlinearity and high-order components of the drag and lift forces. However, as a matter of fact, the oscillating drag force can be directly related to the vortex-shedding pattern in the wake, and the lift force is the key parameter in the vortex-induced-vibration in the cross-flow direction. Gopalkrishnan (1993) calculated the first four harmonics of the oscillating drag force for the three highest amplitudes of oscillation in his study and observed a phenomenon of amplification of the third-order component at high oscillation frequencies. However, his investigations were focused on wall-free cylinders and only the oscillating drag force. Huang and Larsen (2010) and Wang et al. (2013) briefly mentioned the nonlinearity of the oscillating drag force but did not perform further investigations.

In the study described in this paper, the hydrodynamics of a circular cylinder near a wall, oscillating in the transverse direction in a steady current, was experimentally investigated. The first four orders of the oscillating components of the drag and lift forces were calculated separately. The effects of the gap ratio, the oscillation frequency, and the oscillation amplitude on the high-order oscillating drag and lift forces on the cylinder were studied.

Fig. 1. The towing tank.

2. Experimental setup

2.1. Test apparatus

The experiments were performed in a towing tank (Fig. 1), which was 192 m in length, 10 m in width, and 4.2 m in depth. Fig. 2 shows a sketch of the test apparatus. The model was installed in a forced-oscillation facility, which was suspended from the towing carriage together with a plane plate parallel to its axis below it.

The forced-oscillation facility was a combination of horizontal and vertical slider–track systems. The motions of the sliders were driven by servo motors fixed at the end of each track, which could be controlled by software developed by VB.NET.

The plane plate was constructed from stainless steel and had a size of $2.5\ \text{m} \times 2.4\ \text{m} \times 0.003\ \text{m}$ (length × breadth × thickness). It was welded onto a grille to ensure that there would be no deflection due to its weight. The plate was mounted on four steel struts, which were connected to the bottom of the towing carriage. The four thin steel wires hauling the four corners of the plate were anchored to the carriage to prevent vibration of the plate as it moved in the water.

A three-dimensional force transducer was used to measure the forces on the model. We have processed the verification test which shows that the phenomenon of crosstalk between different dimensions can be neglected. The measuring range of the force transducers is ± 150 kg and the precision is 0.1%. Hence the resolution of the force transducers is 0.15 kg, which is acceptable for this experiment compared with the hydrodynamic force of the rigid cylinder.

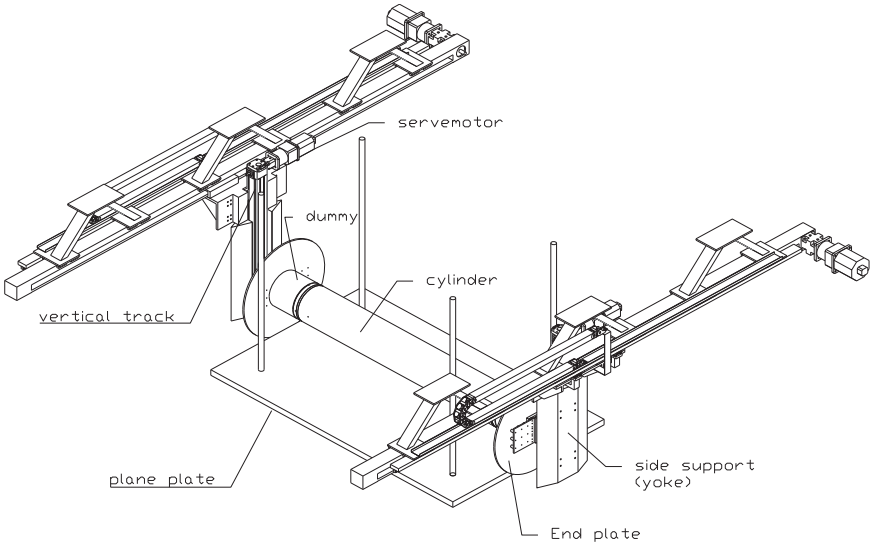

Fig. 2. Schematic of the test apparatus.

An encoder on the servo motor recorded the rotation speed of the motor, which was then transformed into the displacement and velocity of the model. All of the signals representing the force, displacement, and velocity were converted to measurable voltages and recorded synchronously by our software.

Fig. 3 shows a photograph of the experimental apparatus, placed upside down without the plane plate. Many runs were performed in air to examine the accuracy and synchronism of the motion of the cylinder. The two parallel sliders could move synchronously, and the absolute error in the displacements between them was less than 0.5 mm.

2.2. Model

The model was a smooth polypropylene cylinder, 0.25 m in diameter and 2 m in length, implying an aspect ratio $L/D=8$. Two three-dimensional force transducers were attached to the ends of the cylinder to measure the lift and drag forces acting on the model. Fig. 4 shows the arrangement of the model. Two methods were used to eliminate the end boundary effects and the turbulence around the connecting structures at the two ends of the cylinder when it was moving in the water. Firstly, two dummy sections with the same diameter were fixed on the connecting structures as extensions of the cylinder ends, to make sure that the current field encountered by the cylinder was uniform. A small annular clearance of less than 1 mm was maintained between the cylinder and the dummy sections to make sure that the measured forces acted only on the cylinder. Secondly, Perspex circular end plates with a diameter three times larger than that of the model were attached to the ends of the dummy sections to prevent disturbance by the yokes. These two measures guaranteed a nearly two-dimensional flow around the cylinder.

Fig. 3. Model installed in the forced oscillation facility.

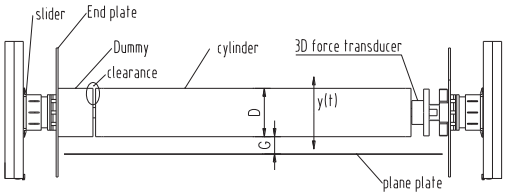

Fig. 4. Arrangement of the model.

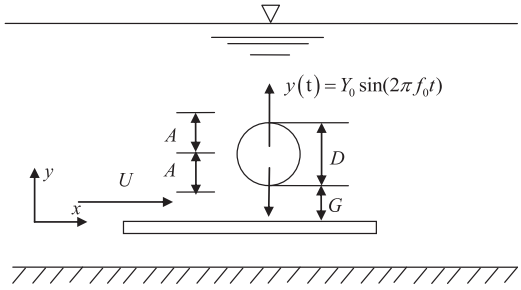

Fig. 5. Sketch defining of some parameters and the coordinate system.

2.3. Experimental procedure

The towing velocity in the study was 0.8 m/s, corresponding to a Reynolds number (based on the cylinder diameter) of approximately 2×10^5. Tests involving forced sinusoidal oscillations of the model cylinder were conducted with different gap ratios G/D ranging from 0.1 to 0.9, with different nondimensional frequencies $\hat{f}_0=f_0D/U$ and amplitudes $Y_0=A/D$. Fig. 5 defines some of the parameters and the coordinate system in the experiment. All of the cases tested are listed in Table 1.

Fig. 6 presents all of the cases tested on a map of vortex-shedding patterns of the kind presented by Williamson and Roshko (1988). Here, the 2S mode corresponds to the classical Kármán wake, with two vortices per cycle of oscillation; the 2P mode corresponds to a pattern with two pairs of vortices per cycle arranged in a staggered fashion on each side of the centerline of the wake; and the P+S mode is an asymmetric pattern with one pair and one single vortex per cycle.

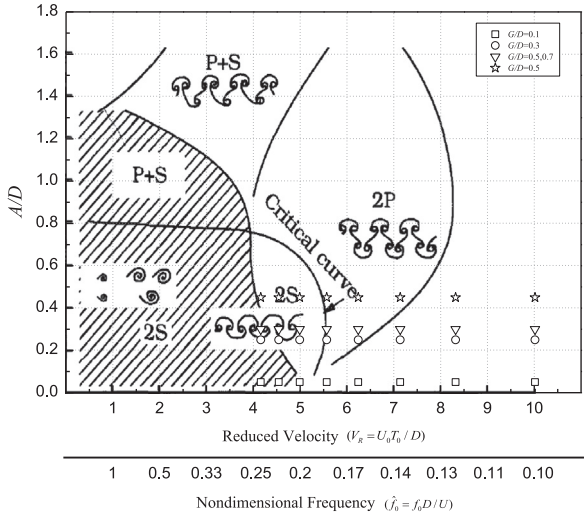

Fig. 6. The cases studied, plotted on the map of vortex shedding patterns.

Table 1
Cases tested in this study.

Nondimensional frequency	0.10	0.12	0.14	0.16	0.18	0.20	0.22	0.24
G/D	Nondimensional amplitude A/D							
0.1	0.05	0.05	0.05	0.05	0.05	0.05	0.05	0.05
0.3	0.25	0.25	0.25	0.25	0.25	0.25	0.25	0.25
0.5	0.3/0.45	0.3/0.45	0.3/0.45	0.3/0.45	0.3/0.45	0.3/0.45	0.3/0.45	0.3/0.45
0.7	0.3	0.3	0.3	0.3	0.3	0.3	0.3	0.3

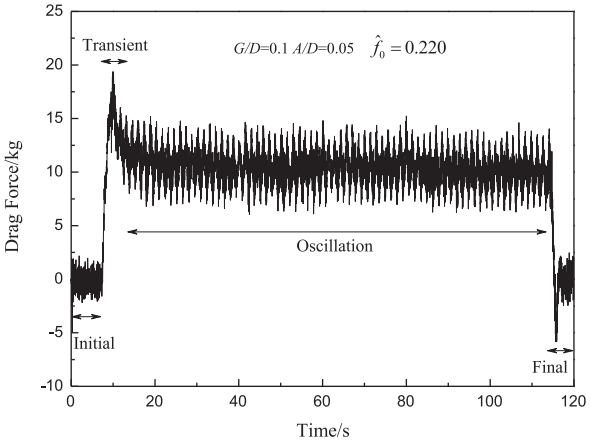

Fig. 7. Trace of drag force for a typical run.

Each experimental run lasted for 120 s. An 8 s initial period was followed by a 3 s period during which a transient occurred, then a 100 s period during which oscillation occurred, and finally a 5 s final period. Fig. 7 illustrates a trace of the drag force for a typical run ($G/D=0.1$, $A/D=0.05$, $\hat{f}_0 = 0.220$).

3. Data processing

When a cylinder oscillates sinusoidally in the cross-flow direction in a steady current, the forces acting on it contain a Strouhal component and an additional oscillating component. If the oscillation is given by

$$y(t) = Y_0 \sin(2\pi f_0 t) \tag{1}$$

where Y_0 is the oscillation amplitude and f_0 is the oscillation frequency, the lift force perpendicular to the flow direction can be expressed as

$$L = L_m + \sum_{n=1}^{k} L_{o\_n} \sin(2\pi(nf_0)t + \phi_n) + L_S \sin(2\pi f_S t + \phi_S) \tag{2}$$

where L_m is the mean lift force, L_{o_n} and ϕ_n are the magnitude and phase angle of the oscillating lift force at the frequency nf_0, and L_S and ϕ_S are the magnitude and phase angle of the Strouhal lift force. In this paper, we focus on the first four orders of the force components, and so $k=4$.

In the flow direction, the drag force can be expressed as

$$D = D_m + \sum_{n=1}^{k} D_{o\_n} \sin(2\pi(nf_0)t + \psi_n) + D_S \sin(2\pi(2f_S)t + \psi_S) \tag{3}$$

where D_m is the mean drag force, D_{o_n} and ψ_n are the magnitude and phase angle of the oscillating drag force at nf_0, and D_S and ψ_S are the magnitude and phase angle of the Strouhal drag force. As the component at the oscillation frequency will completely dominate the force on an oscillating cylinder, the Strouhal component can be neglected in both Eqs. (2) and (3). Therefore, each of the force components in Eqs. (2) and (3) can be nondimensionalized, and then the lift coefficient can be expressed as

$$C_L = C_{L_m} + \sum_{n=1}^{4} C_{L_{o\_n}} \sin(2\pi(nf_0)t + \phi_n) \tag{4}$$

The drag coefficient can be expressed as

$$C_D = C_{D_m} + \sum_{n=1}^{4} C_{D_{o\_n}} \sin(2\pi(nf_0)t + \psi_n) \tag{5}$$

where C_{L_m} and C_{D_m} are the mean lift and drag coefficients, and $C_{L_{o\_n}}$ and $C_{D_{o\_n}}$ are the magnitudes of the oscillating lift and drag coefficients at nf_0, as shown in Fig. 7.

A waveform $x(t)$ can be expressed as a Fourier series as follows:

$$x(t) = a_0 + \sum_{n=1}^{\infty} a_n \cos\left(\frac{2\pi nt}{T}\right) + \sum_{n=1}^{\infty} b_n \sin\left(\frac{2\pi nt}{T}\right) \tag{6}$$

where the coefficients a_0, a_n, and b_n are given by

$$a_0 = \frac{1}{T}\int_t^{t+T} x(t)dt \tag{7}$$

$$a_n = \frac{2}{T}\int_t^{t+T} x(t)\cos\left(\frac{2\pi nt}{T}\right)dt \tag{8}$$

$$b_n = \frac{2}{T}\int_t^{t+T} x(t)\sin\left(\frac{2\pi nt}{T}\right)dt \tag{9}$$

The symbol n refers to which multiple of the oscillation frequency f_0 the coefficient is calculated for.

For the lift coefficient,

$$C_{L_{o\_n}} = \sqrt{a_n^2 + b_n^2} \tag{10}$$

$$\phi_n = \arctan\left(\frac{a_n}{b_n}\right) \tag{11}$$

Using the values of $C_{L_{o\_n}}$ and ϕ_n obtained from Eqs. (10) and (11), the oscillating lift coefficient can be decomposed as shown in Fig. 8. And Fig. 9 shows a vector diagram of the oscillation of the cylinder, and of the velocity, acceleration, and lift force, where the lift coefficient in phase with the velocity is

$$C_{L\_V_n} = C_{L_{o\_n}} \sin\phi_n \tag{12}$$

The lift coefficient in phase with the acceleration is

$$C_{L\_A_n} = C_{L_{o\_n}}(-\cos\phi_n) \tag{13}$$

For the drag coefficient,

$$C_{D_m} = a_0 \tag{14}$$

$$C_{D_{o\_n}} = \sqrt{a_n^2 + b_n^2} \tag{15}$$

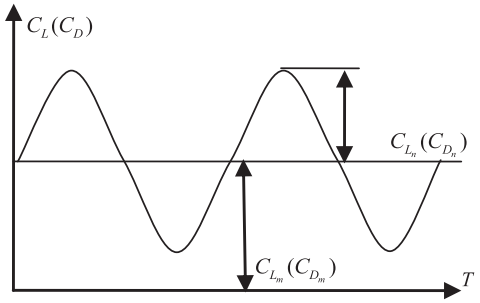

Fig. 8. Mean and oscillating lift and drag coefficients.

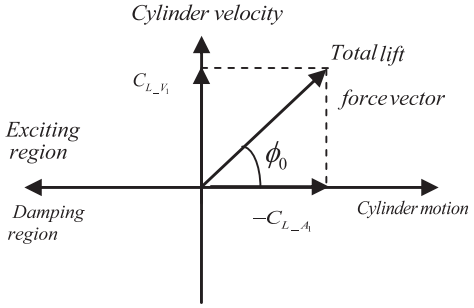

Fig. 9. Vector diagram of the cylinder oscillation, velocity, acceleration and lift force.

4. Results and discussion

4.1. Oscillating drag coefficient

Figs. 10–13 show the magnitudes of the first four orders of the oscillating drag coefficient for four different gap ratios against the nondimensional frequency. For all four gap ratios, the magnitudes of the four orders decrease with increasing order, that is, $C_{D_{o\_1}} > C_{D_{o\_2}} > C_{D_{o\_3}} > C_{D_{o\_4}}$. $C_{D_{o\_3}}$ and $C_{D_{o\_4}}$ are much smaller than $C_{D_{o\_1}}$ and $C_{D_{o\_2}}$ in the high-frequency region, but very close to them in the low-frequency region, especially for small gap ratios. In addition, $C_{D_{o\_3}}$ and $C_{D_{o\_4}}$ show similar trends as the nondimensional frequency increases, and they both reach a peak at the lock-in frequency and show amplification at high frequency, but the variation of the amplitude is much more gentle than for the first two orders.

To show the proportions of the first four orders in the whole oscillating drag coefficient for further analysis, we plotted the corresponding percentage figures. The percentage of each order was calculated from

$$\text{Percentage} = \frac{C_{D/L_{o\_n}}}{C_{D/L_{o\_1}} + C_{D/L_{o\_2}} + C_{D/L_{o\_3}} + C_{D/L_{o\_4}}} \tag{16}$$

The percentage of the first-order oscillating drag coefficient $C_{D_{o\_1}}$ is shown in Fig. 14 against the nondimensional frequency for different gap ratios. The proportion of $C_{D_{o\_1}}$ decreases slightly with increasing G/D, which means that the existence of $C_{D_{o\_1}}$ may be caused by the asymmetry of the vortex-shedding process due to the near wall. Naturally, the effect of the wall will become weaker as the wall becomes further away from the cylinder, and then $C_{D_{o\_1}}$ will decrease. The proportion of $C_{D_{o\_1}}$ increases slightly with increasing nondimensional frequency for each value of G/D.

The percentage of the second-order oscillating drag coefficient $C_{D_{o\_2}}$ is shown in Fig. 15 against the nondimensional frequency. The proportion of $C_{D_{o\_2}}$ increases with increasing G/D, but does not

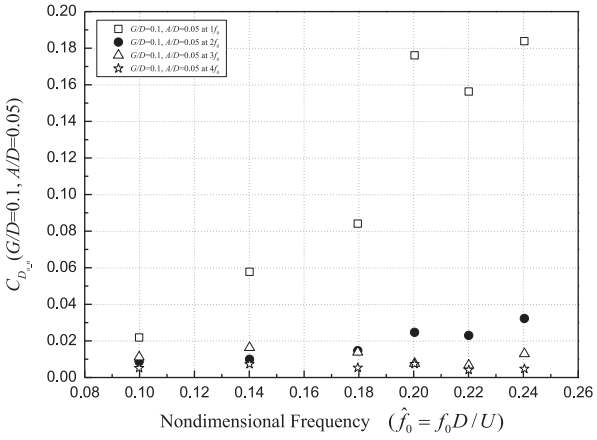

Fig. 10. Magnitudes of the first four orders of the oscillating drag coefficient magnitudes (G/D=0.1, A/D=0.05).

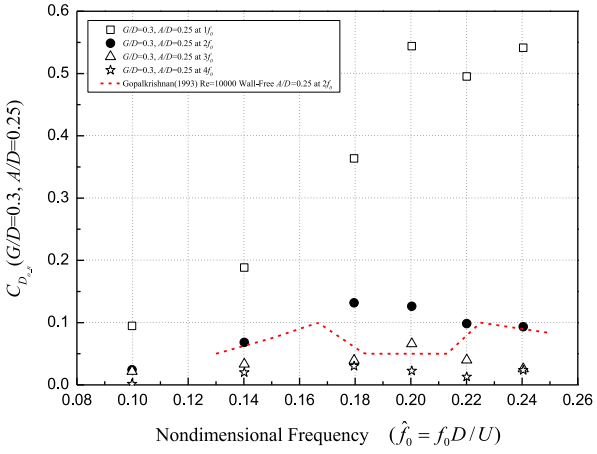

Fig. 11. Magnitudes of the first four orders of the oscillating drag coefficient magnitudes (G/D=0.3, A/D=0.25).

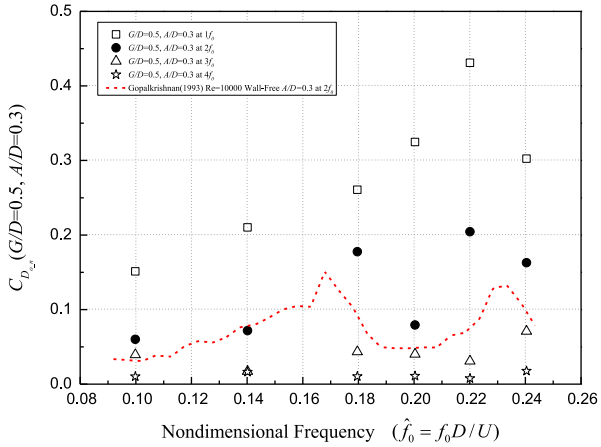

Fig. 12. Magnitudes of the first four orders of the oscillating drag coefficient magnitudes (G/D=0.5, A/D=0.3).

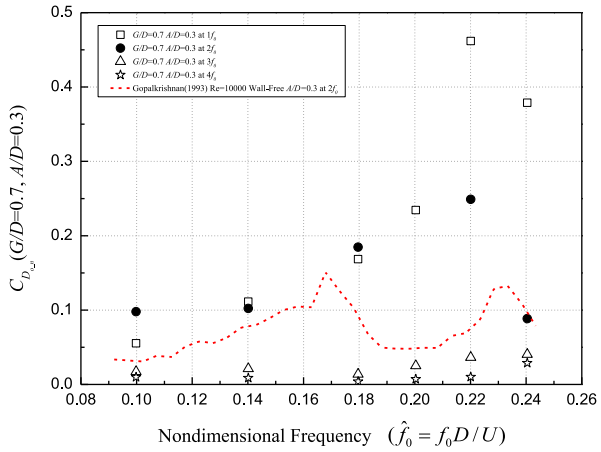

Fig. 13. Magnitudes of the first four orders of the oscillating drag coefficient magnitudes (G/D=0.7, A/D=0.3).

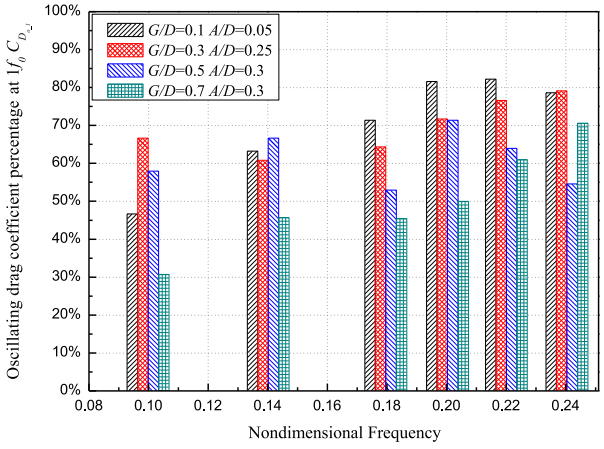

Fig. 14. Percentage of oscillating drag coefficient percentage at $1f_0$.

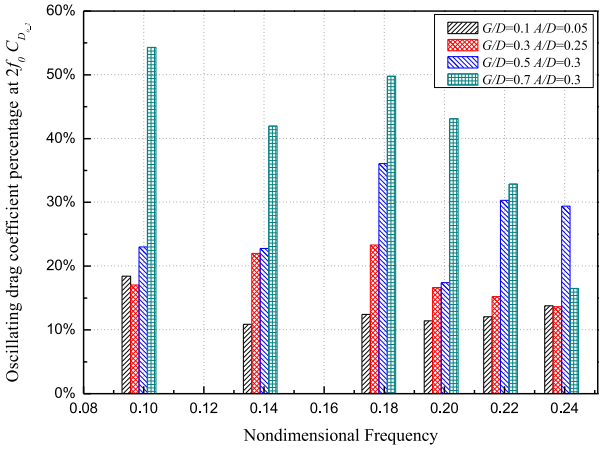

Fig. 15. Percentage of oscillating drag coefficient percentage at $2f_0$.

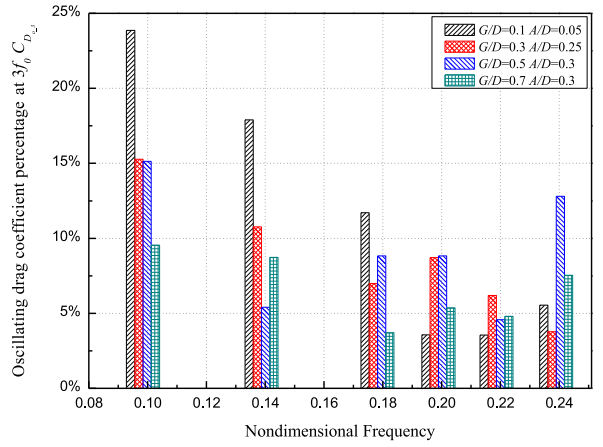

Fig. 16. Percentage of oscillating drag coefficient percentage at $3f_0$.

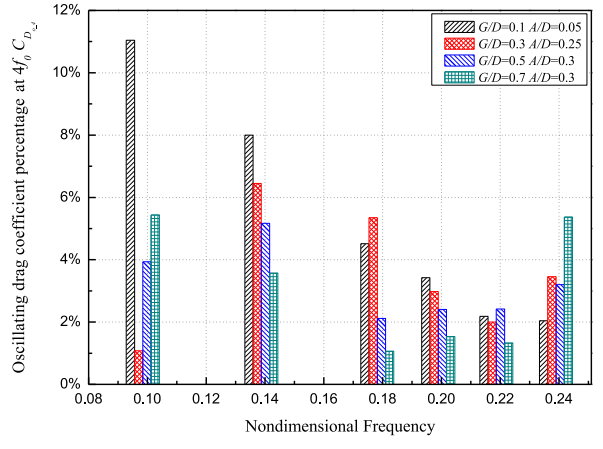

Fig. 17. Percentage of oscillating drag coefficient percentage at $4f_0$.

have much variation with the nondimensional frequency at any given value of G/D.

The percentage of the third-order oscillating drag coefficient $C_{D_{o\_3}}$ is shown in Fig. 16 against the nondimensional frequency. The proportion of $C_{D_{o\_3}}$ decreases with increasing nondimensional frequency. For $G/D=0.1$, 0.3, and 0.5, which correspond to positions very near the wall, the proportion of $C_{D_{o\_3}}$ can be comparable to that of $C_{D_{o\_2}}$.

The percentage of the fourth-order oscillating drag coefficient $C_{D_{o\_4}}$ is shown in Fig. 17 against the nondimensional frequency. Basically, the proportion of $C_{D_{o\_4}}$ decreases with increasing nondimensional frequency.

Comparing the four figures (Figs. 14–17), it can be clearly seen that the proportion of each order $C_{D_{o\_n}}$ decreases with increasing order. At each value of G/D, the variation of the proportions of the four orders of the oscillating drag coefficient with increasing nondimensional frequency is as follows: $C_{D_{o\_1}}$ increases, $C_{D_{o\_3}}$ and $C_{D_{o\_4}}$ decrease, and $C_{D_{o\_2}}$ remains almost constant, which means that the nondimensional frequency has a much larger influence on $C_{D_{o\_1}}$.

Four typical time histories of combinations of different orders of the oscillating drag coefficient are shown in Figs. 18–21, which demonstrate the different effects of the different orders.

Figs. 18 and 19 show the time histories of different combinations of orders of the oscillating drag coefficient for $G/D=0.3$. In Fig. 18, the nondimensional frequency $\hat{f}_0$ equals 0.1. An obvious variation in the time series is witnessed when $C_{D_{o\_3}}$ is added to the curve of $C_{D_{o\_1}}+C_{D_{o\_2}}$; this result agrees with the conclusion drawn above, namely that $C_{D_{o\_3}}$ accounts for a large proportion in the low-frequency region for small G/D. In addition, it can be clearly seen that $C_{D_{o\_4}}$ has nearly no influence on the curve, which also agrees with the results presented above. In Fig. 19, the nondimensional frequency $\hat{f}_0$ equals 0.24. In this case, no large variation in the waveform is observed when high-order coefficients are added; this is because the proportion of $C_{D_{o\_1}}$ is nearly 80% and the influence of the other orders is negligible.

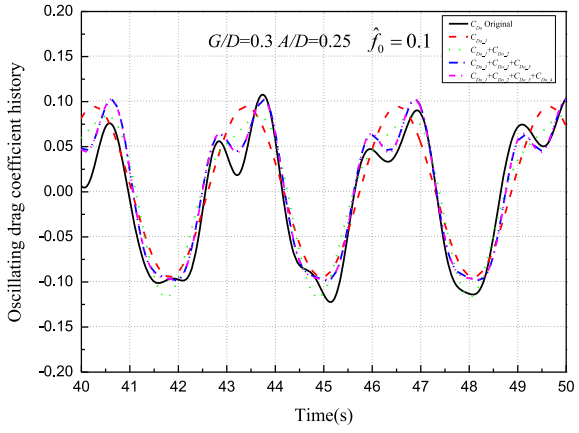

Fig. 18. Time history of scillating drag coefficient history at $G/D=0.3$, $A/D=0.25$ and $\hat{f}_0=0.1$.

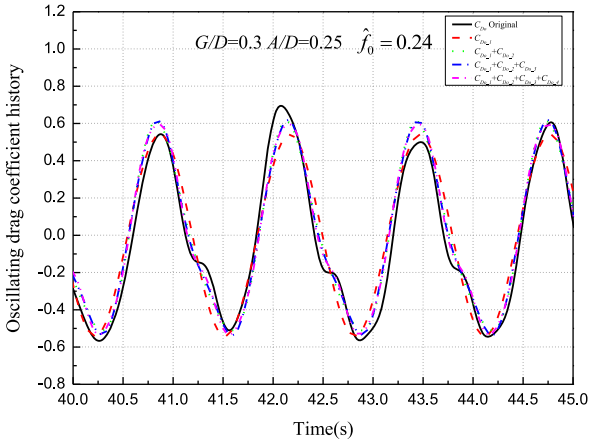

Fig. 19. Time history of scillating drag coefficient history at $G/D=0.3$, $A/D=0.25$ and $\hat{f}_0=0.24$.

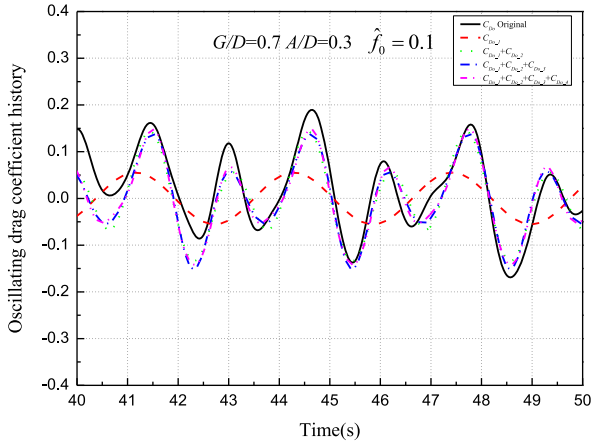

Fig. 20. Time history of scillating drag coefficient history at $G/D=0.7$, $A/D=0.3$ and $\hat{f}_0 = 0.1$.

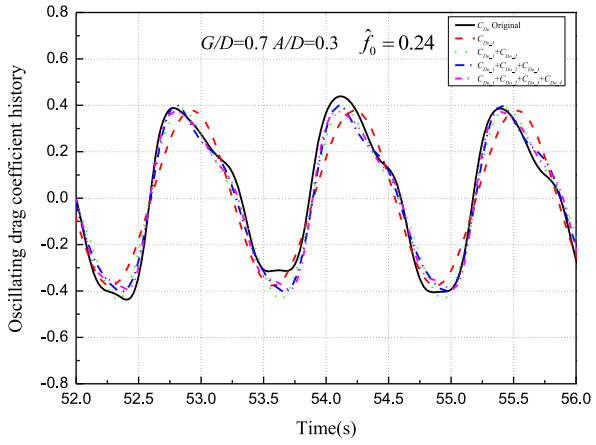

Fig. 21. Time history of scillating drag coefficient history at $G/D=0.7$, $A/D=0.3$ and $\hat{f}_0 = 0.24$.

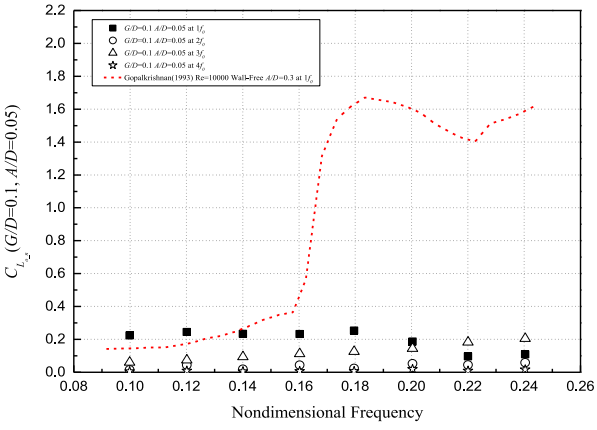

Fig. 22. Magnitudes of the first four orders of the oscillating lift coefficient magnitudes ($G/D=0.1$, $A/D=0.05$).

Figs. 20 and 21 show the time histories of different combinations of orders of the oscillating drag coefficient for $G/D=0.7$. Similarly to the case of $G/D=0.3$, the effect of the high-order components is much more obvious at $\hat{f}_0 = 0.1$ than at $\hat{f}_0 = 0.24$. At $\hat{f}_0 = 0.1$, the waveform changes dramatically when $C_{D_{o\_2}}$ is added to $C_{D_{o\_1}}$, but no obvious changes are observed when the remaining two orders are added to $C_{D_{o\_1}} + C_{D_{o\_2}}$. It is thus clear that the proportion of $C_{D_{o\_2}}$ for $G/D=0.7$ is larger than that for $G/D=0.3$, which also confirms that the proportion of $C_{D_{o\_2}}$ increases with increasing G/D.

4.2. Oscillating lift coefficient

Figs. 22–25 show the magnitudes of the first four orders of the oscillating lift coefficient for different gap ratios against the nondimensional frequency. In Fig. 22, where $G/D=0.1$, the vortex-shedding

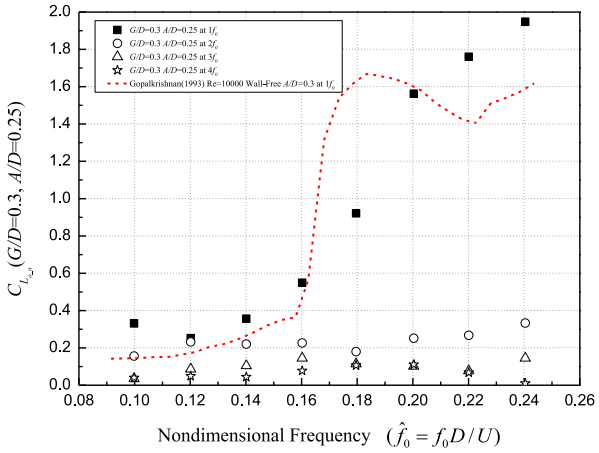

Fig. 23. Magnitudes of the first four orders of the oscillating lift coefficient magnitudes ($G/D=0.3$, $A/D=0.25$).

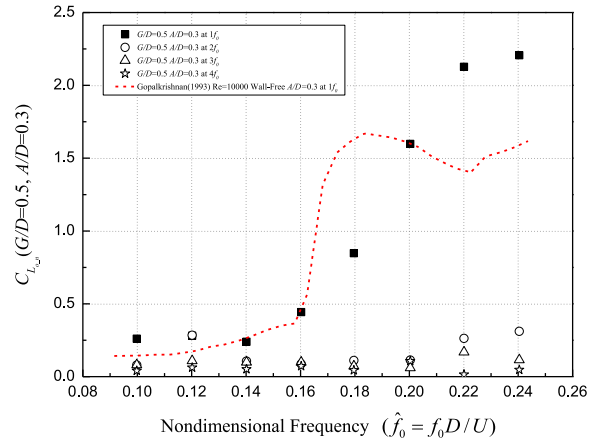

Fig. 24. Magnitudes of the first four orders of the oscillating lift coefficient magnitudes ($G/D=0.5$, $A/D=0.3$).

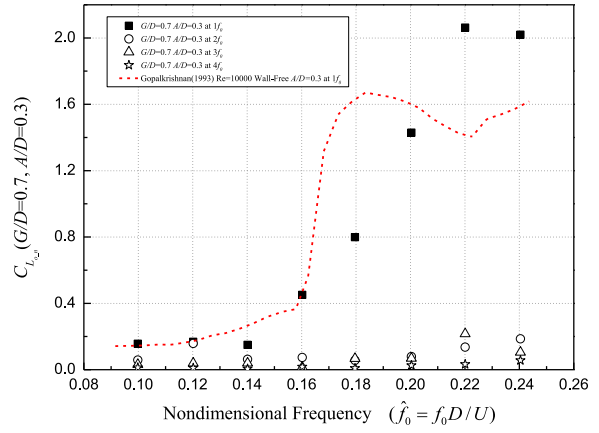

Fig. 25. Magnitudes of the first four orders of the oscillating lift coefficient magnitudes ($G/D=0.7$, $A/D=0.3$).

process is almost suppressed, and the basic pattern is $C_{L_{o\_1}} > C_{L_{o\_3}} > C_{L_{o\_2}} > C_{L_{o\_4}}$, except in the high-frequency region, where $C_{L_{o\_3}} > C_{L_{o\_1}}$. With increasing nondimensional frequency, $C_{L_{o\_1}}$ decreases when $\hat{f}_0 > 0.18$, $C_{L_{o\_3}}$ increases slowly, and $C_{L_{o\_2}}$ and $C_{L_{o\_4}}$ remain almost constant.

In the cases where $G/D=0.3$, 0.5, and 0.7, as shown in Figs. 23, 24 and 25, respectively, the trends observed are similar to those of the oscillating drag coefficient. The four orders of the oscillating lift coefficient decrease with increasing order, that is, $C_{L_{o\_1}} > C_{L_{o\_2}} > C_{L_{o\_3}} > C_{L_{o\_4}}$. $C_{L_{o\_2}}$ and $C_{L_{o\_3}}$ are much smaller than $C_{L_{o\_1}}$ in the high-frequency region, but they are very close to $C_{L_{o\_1}}$ in the low-frequency region. With increasing nondimensional frequency, $C_{L_{o\_2}}$ reaches a peak around $\hat{f}_0 = 0.12$ and also gradually increases in the high-frequency region, $C_{L_{o\_3}}$ shows amplification in the high-frequency region, but $C_{L_{o\_4}}$ remains almost constant.

The percentage of the first-order oscillating lift coefficient $C_{L_{o\_1}}$ is shown in Fig. 26 against the nondimensional frequency. With increasing nondimensional frequency, the proportion of $C_{L_{o\_1}}$ decreases in the case of $G/D=0.1$ and increases for other values of G/D. The proportion of $C_{L_{o\_1}}$ increases with increasing G/D for $G/D=0.3$, 0.5, and 0.7.

The percentage of the second-order oscillating lift coefficient $C_{L_{o\_2}}$ is shown in Fig. 27 against the nondimensional frequency. For $G/D=0.3$, 0.5, and 0.7, the proportion of $C_{L_{o\_2}}$ reaches about 40% at $\hat{f}_0 = 0.12$, which is very close to that of $C_{L_{o\_1}}$, then decreases rapidly with increasing nondimensional frequency, and reaches stability in the high-frequency region. The proportion of $C_{L_{o\_2}}$ increases with increasing G/D in the high-frequency region.

The percentages of the third- and fourth-order oscillating lift coefficients $C_{L_{o\_3}}$ and $C_{L_{o\_4}}$ are shown in Figs. 28 and 29 against the nondimensional frequency. It can be seen that in the cases of $G/D=0.3$, 0.5, and 0.7, the proportions of $C_{L_{o\_3}}$ and $C_{L_{o\_4}}$ decrease with increasing nondimensional frequency and are only about 15% in total in the high-frequency region, which means that they are negligible. But in the case of $G/D=0.1$, the proportion of $C_{L_{o\_3}}$ increases rapidly and exceeds 50% when the nondimensional frequency is larger than 0.22.

Comparing the four figures (Figs. 26–29), it can be clearly seen that the proportion of each order of $C_{L_{o\_n}}$ decreases with increasing order. Moreover, in each case except for $G/D=0.1$, with increasing nondimensional frequency, the proportion of $C_{L_{o\_1}}$ increases and the other three proportions decrease, which indicates that an increase in the nondimensional frequency has a stronger influence on $C_{L_{o\_1}}$.

Figs. 30–33 show the time histories of different combinations of different orders of the oscillating lift coefficient for $G/D=0.3$ and 0.7. In Figs. 30 and 32, for a nondimensional frequency $\hat{f}_0 = 0.1$, an obvious variation in the time series is witnessed when $C_{L_{o\_2}}$ is added to $C_{L_{o\_1}}$; this is because the proportion of $C_{L_{o\_2}}$ is about 20%, which is about one third of that of $C_{L_{o\_1}}$. However, in Figs. 31 and 33, for a nondimensional frequency $\hat{f}_0 = 0.24$, all of the orders other than the first are negligible.

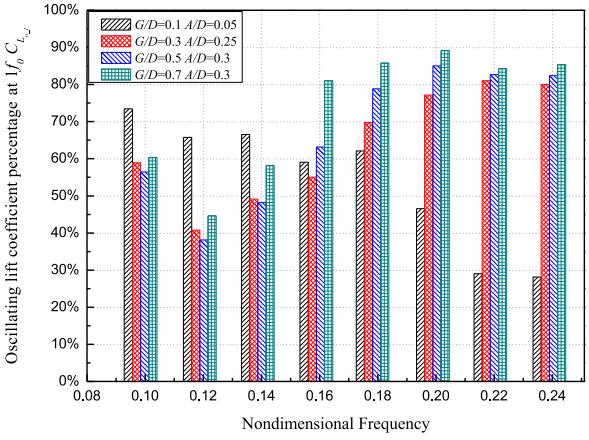

Fig. 26. Percentage of oscillating lift coefficient percentage at $1f_0$.

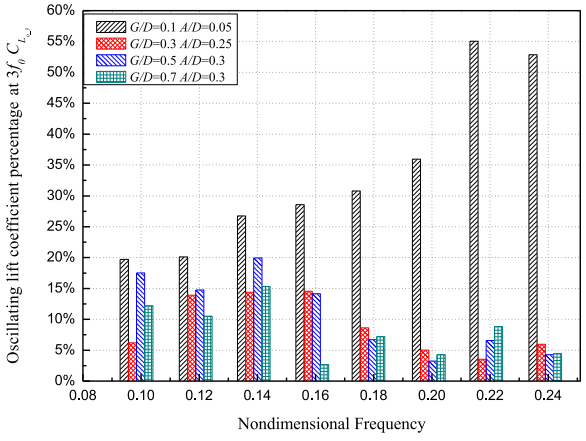

Fig. 28. Percentage of oscillating lift coefficient percentage at $3f_0$.

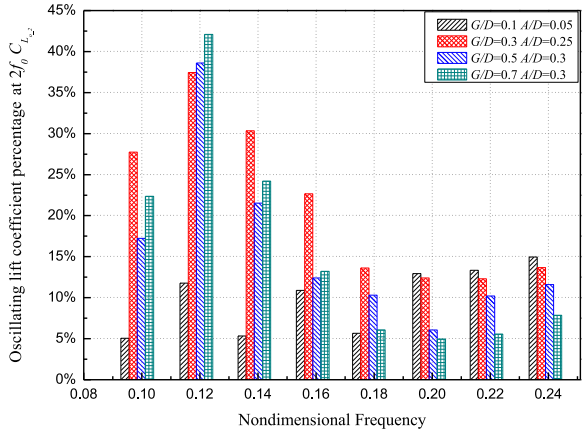

Fig. 27. Percentage of oscillating lift coefficient percentage at $2f_0$.

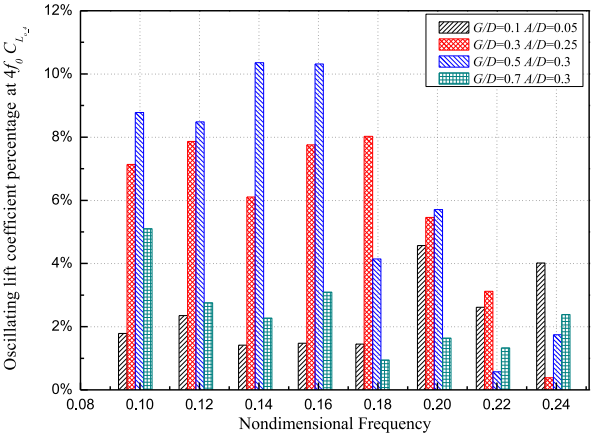

Fig. 29. Percentage of oscillating lift coefficient percentage at $4f_0$.

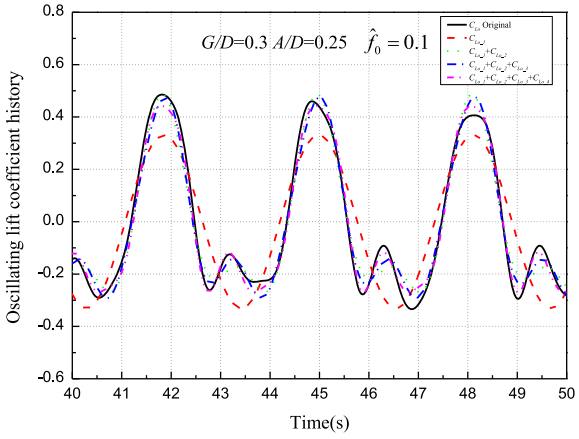

Fig. 30. Time history of oscillating lift coefficient history at $G/D=0.3$, $A/D=0.25$ and $\hat{f}_0 = 0.1$.

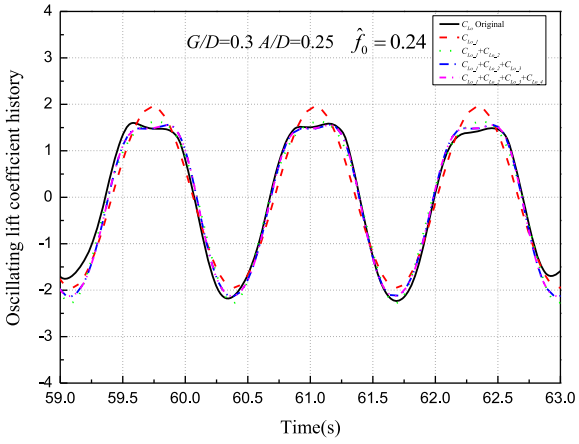

Fig. 31. Time history of scillating lift coefficient history at $G/D=0.3$, $A/D=0.25$ and $\hat{f}_0 = 0.24$.

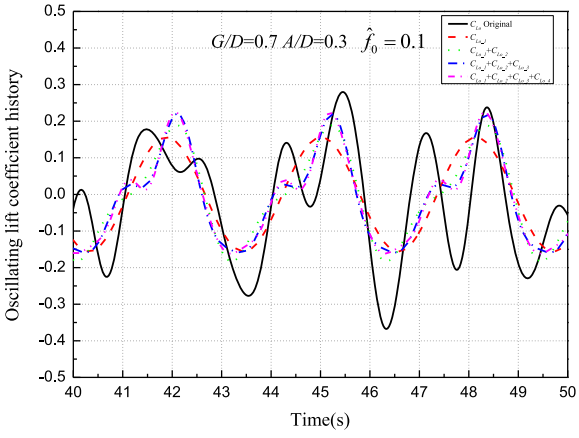

Fig. 32. Time history of scillating lift coefficient history at $G/D=0.7$, $A/D=0.3$ and $\hat{f}_0 = 0.1$.

4.3. *Effect of oscillation amplitude*

Figs. 34 and 35 illustrate the effects of the oscillation amplitude on the various orders of the oscillating drag and lift coefficients. As shown, each order of $C_{D_{o\_n}}$ and $C_{L_{o\_n}}$ increases with increasing oscillation amplitude. As the cylinder approaches the wall, a sudden decrease in the gap occurs, which leads to a high flow

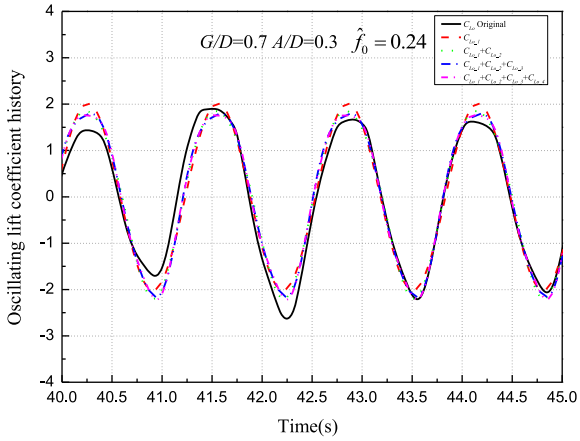

Fig. 33. Time history of scillating lift coefficient history at $G/D=0.7$, $A/D=0.3$ and $\hat{f}_0 = 0.24$.

velocity on the side of the cylinder near the wall, and hence the pressure on that side of the cylinder is reduced, resulting in an extremely high lift force. The larger the amplitude becomes, the smaller the gap becomes, and hence the corresponding coefficients increase. This pattern of increase is similar for every order of the coefficients.

The percentages of the four orders $C_{D_{o\_n}}$ of the oscillating drag coefficient are shown in Fig. 36 for $G/D=0.5$ and different oscillation amplitudes. As shown, the variations of the proportions of $C_{D_{o\_n}}$ as the oscillation amplitude is increased from 0.3 to 0.45 are as follows: $C_{D_{o\_1}}$ and $C_{D_{o\_2}}$ decrease, while $C_{D_{o\_3}}$ and $C_{D_{o\_4}}$ increase. So, it can be clearly seen that a large amplitude has a stronger influence on the higher orders $C_{D_{o\_n}}$, especially $C_{D_{o\_4}}$.

For the oscillating lift coefficient, as shown in Fig. 37, the variation of $C_{L_{o\_n}}$ as the oscillation amplitude is increased from 0.3 to 0.45, is not as significant as that of $C_{D_{o\_n}}$, which means that the effects of the oscillation amplitude on $C_{L_{o\_n}}$ are weaker than those on $C_{D_{o\_n}}$. In the high-frequency region, the proportion of $C_{L_{o\_1}}$ decreases and that of $C_{L_{o\_2}}$ increases, and the variation of the oscillation amplitude has the strongest influence on $C_{L_{o\_2}}$ in the four orders of the oscillating lift coefficient.

5. Conclusions

In this study, the hydrodynamics of a circular cylinder oscillating in the transverse direction in a steady current near a wall was experimentally investigated. The first four orders of the oscillating components of the drag and lift forces acting on the cylinder were calculated separately. The effects of the gap ratio, the oscillation frequency, and the oscillation amplitude on the high-order components of these forces were analyzed. The following conclusions can be drawn.

5.1. *Oscillating drag coefficient*

1. The existence of a nearby wall results in the appearance of a first-order oscillating drag coefficient, which has not been found in wall-free forced-oscillation tests. The magnitude and proportion of the first-order oscillating drag coefficient decrease with increasing G/D.
2. In general, the magnitudes and proportions of the first four orders of the oscillating drag coefficient decrease with increasing order. The magnitudes of the third and fourth orders are very small but still account for a large proportion of the total coefficient in the low-frequency region for small G/D; therefore, they cannot be considered as negligible.

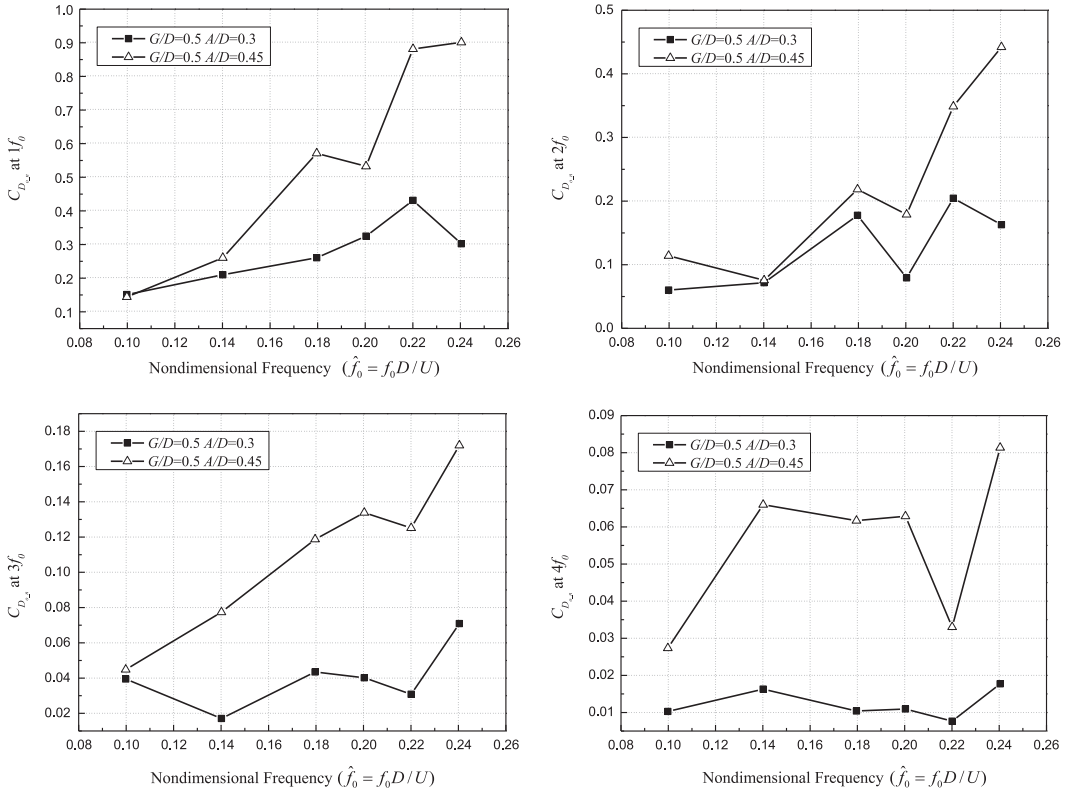

Fig. 34. Magnitude of oscillating drag coefficient for $G/D=0.5$ and different oscillation amplitudes.

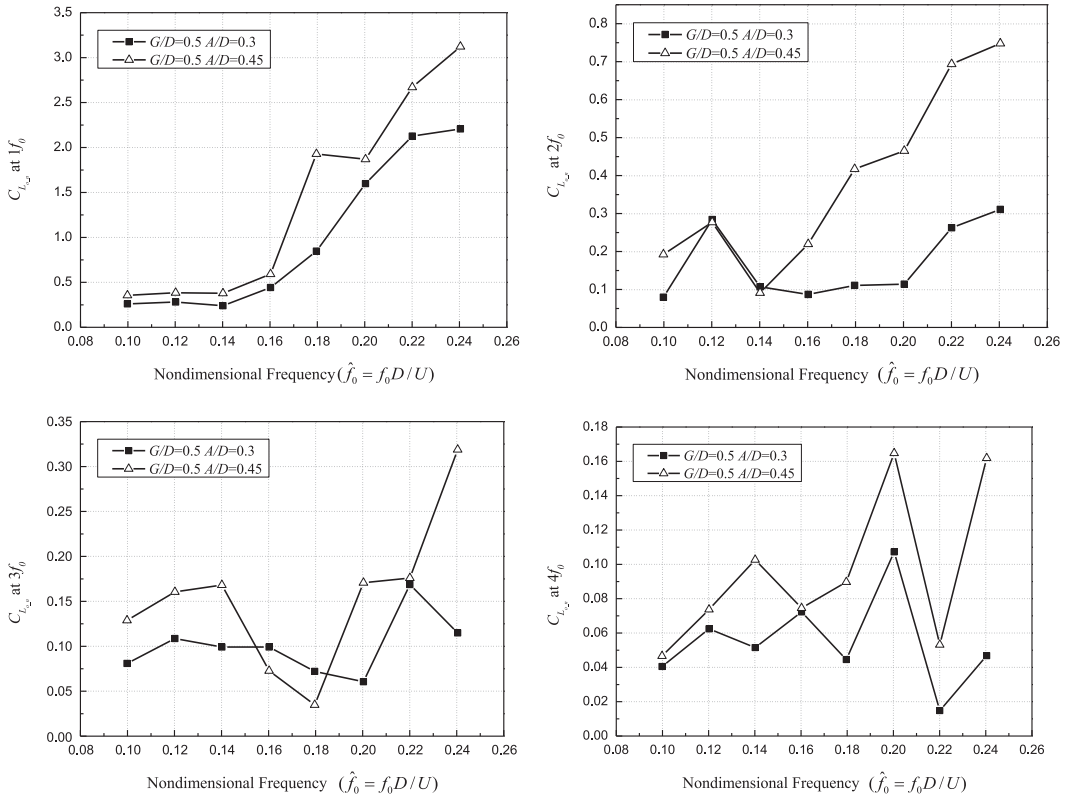

Fig. 35. Magnitude of oscillating lift coefficient for $G/D=0.5$ and different oscillation amplitudes.

3. For each value of G/D, the magnitudes of the third- and fourth-order oscillating drag coefficients increase slightly in the lock-in region, and the third order also increases in the high-frequency region. An increase in the nondimensional frequency has a much stronger influence on the first-order oscillating drag coefficient than on the others.

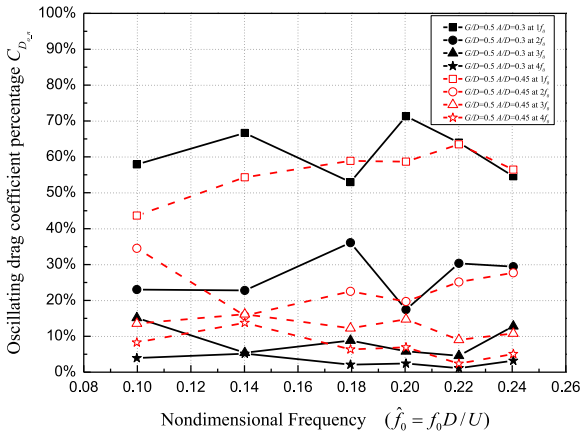

Fig. 36. Percentages of oscillating drag coefficient percentage for $G/D=0.5$ and different oscillating amplitudes.

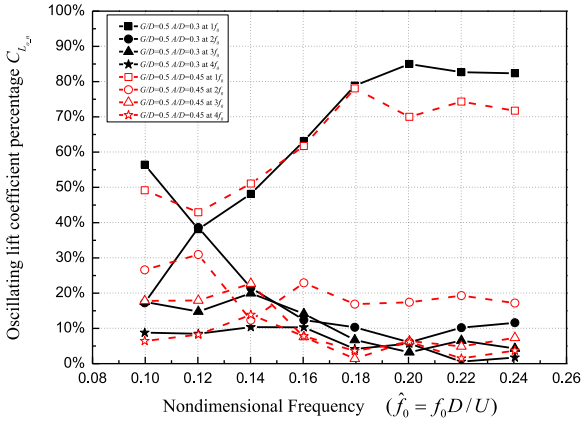

Fig. 37. Percentages of oscillating lift coefficient percentage for $G/D=0.5$ and different oscillating amplitudes.

5.2. *Oscillating lift coefficient*

1. In general, the magnitudes and proportions of the first four orders of the oscillating lift coefficient decrease with increasing order. The magnitudes of the second, third, and fourth orders are very small, but the second order can still account for a proportion of 40% in the low-frequency region; therefore, they cannot be considered as negligible.
2. For each value of G/D, an increase in the nondimensional frequency has a much stronger influence on the first-order oscillating lift coefficient than on the others.

5.3. *Effect of oscillation amplitude*

The magnitudes of all orders of the oscillating drag and lift coefficients increase with increasing oscillation amplitude, especially in the case of the fourth-order oscillating drag coefficient and the second-order oscillating lift coefficient. However, the effects of the oscillation amplitude on the oscillating lift coefficient are insignificant compared with those on the oscillating drag coefficient.

Acknowledgments

Financial support from the Natural Science Foundation of China (Grant nos. 51009088 and 51279101) is gratefully acknowledged.

References

Bearman, P.W., Zdravkovich, M.M., 1978. Flow around a circular cylinder near a plane boundary. Journal of Fluid Mechanics 89 (1), 33–47.
Bishop, R.E.D., Hassan, A.Y., 1964. The lift and drag forces on a circular cylinder oscillating in a flowing fluid. Proceedings of the Royal Society of London Part A 277, 51–57.
Buresti, G., Lanciotti, A., 1992. Mean and fluctuating forces on a circular cylinder in cross-flow near a plane surface. Wind Engineering and Industrial Aerodynamics 41 (1-3), 639–650.
Carberry, J., Sheridan, J., Rockwell., D., 2005. Controlled oscillations of a cylinder: forcesand wake modes. Journal of Fluid Mechanics 538, 31–69.
Gopalkrishnan, R., 1993. Vortex Induced Forces on Oscillating Bluff Cylinders (Ph.D. thesis). Department of Ocean Engineering, MIT, Cambridge, MA, USA.
Grass, A.J., Raven, P.W.J., Stuart, R.J., Bray, J.A., 1984. The influence of boundary layer velocity gradients and bed proximity on vortex shedding from free spanning pipelines. ASME Journal of Energy Resources Technology 106, 70–78.
Huang, Z.Y., Larsen, C.M., 2010. Large eddy simulation of an oscillating cylinder close to a wall. In: Proceedings of the ASME 2010 29th International Conference on Ocean, Offshore and Arctic Engineering, Shanghai.
Lei, C., Cheng, L., Kavanagh, K., 1999. Re-examination of the effect of a plane boundary on force and vortex shedding of a circular cylinder. Journal of Wind Engineering and Industrial Aerodynamics 80 (3), 263–286.
Nishino, T., Roberts, G.T., Zhang, X., 2007. Vortex shedding from a circular cylinder near a moving ground. Physics of Fluid 19, 025103.
Roshko A., Steinolfson A., Chattoorgoon V., 1975. Flow forces on a cylinder near a wall or near another cylinder. Proceedings of the 2nd U.S. National Conference on Wind Engineering Research, Colorado State University, Fort Collins, paper IV-15.
Sarpkaya, T., 1978. Fluid forces on oscillating cylinders. ASCE Journal of Waterway, Port, Coastal and Ocean Division 104, 275–290.
Sarpkaya, T., 2004. A critical review of the intrinsic nature of vortex-induced vibrations. Journal of Fluids and Structures 19, 389–447.
Sumer, B.M., Fredsoe, J., Jensen, B.L., Christiansen, N., 1994. Forces on vibrating cylinder near wall current and waves. Journal of Waterway Port Coastal and Ocean Engineering–ASCE 120 (03), 233–250.
Wang, X.K., Hao, Z., Tan, S.K., 2013. Vortex-induced vibrations of a neutrally buoyant circular cylinder near a plane wall. Journal of Fluids and Structures 39, 188–204.
Williamson, C.H.K., Roshko, A., 1988. Vortex formation in the wake of an oscillating cylinder. Journal of Fluids and Structures 2, 355–381.
Yang, B., Gao, F.P., Jeng, D.S., Wu, Y.X., 2007. Experimental study of vortex-induced vibrations of a pipeline near an erodible sandy seabed. Ocean Engineering 35, 301–309.
Zdravkovich, M.M., 1985. Forces on a circular cylinder near a plane wall. Applied Ocean Research 7 (4), 197–201.
Zhao, M., Cheng, L., 2011. Numerical simulation of two-degree-of-freedom vortex-induced vibration of a circular cylinder close to a plane boundary. Journal of Fluids and Structures 27, 1097–1110.